


Predicting the outcome of collisional neutrino flavor conversion

Julien Froustey  ^{1,2,*}

¹*Department of Physics, University of California Berkeley, Berkeley, CA 94720, USA*

²*Department of Physics, University of California San Diego, La Jolla, CA 92093, USA*

Collisional flavor instabilities, driven by differing neutrino and antineutrino reaction rates, are expected to occur in dense astrophysical environments like supernovae and neutron star mergers, but have yet to be incorporated in large-scale simulations. We derive, for the first time, analytical expressions for the asymptotic state resulting from a homogeneous and isotropic instability, and apply these predictions to two representative conditions from a neutron star merger simulation. We emphasize the importance of using a collision term that allows for both damping of flavor coherence and relaxation back to thermal equilibrium, which leads to a “quantum” equilibrium with nonzero coherence. These results can be implemented in a subgrid model of collisional flavor transformation, an important step toward the inclusion of flavor oscillation physics into global simulations.

In our current era of multi-messenger astronomy, significant efforts are underway to model dense astrophysical objects such as core-collapse supernovae (CCSNe) or binary neutron star mergers (NSMs), with large-scale simulations incorporating a wide range of physics, including (magneto)hydrodynamics, general relativity, or the nuclear equation of state (see [1–6] and references therein). A key ingredient in all simulations is neutrino transport [7–10] yet to date, neutrino oscillations are not systematically taken into account. Over the last decades, however, various flavor transformation mechanisms have been identified, which are expected to occur in these environments and may have important consequences on the dynamics (see, e.g., [11–18] for reviews).

A direct approach, solving the “quantum” version of Boltzmann’s equation describing neutrino transport with flavor mixing—the Quantum Kinetic Equation (QKE)—, is made unfeasible by the vast differences of length- and time-scales involved. Nevertheless, to assess the potential consequences of neutrino flavor oscillations, simplified models have been used in CCSNe [19–22], post-merger accretion disks [23–25] and recently a full NSM simulation [26]. Other techniques, designed to mitigate the computational cost of a full multi-angle QKE treatment, include an attenuation of the QKE Hamiltonian [27–30], or the use of angular moments of the neutrino density matrix [31–36]. A convenient approach that can be embedded in classical simulations consists in designing a *subgrid model* of flavor transformation [37], which requires one to determine the state reached by the system post-flavor conversion. This has been heavily studied for fast flavor instabilities (FFIs), establishing that the final quasi-steady state is characterized by some cancellation of the angular crossing between (anti)neutrino distributions, which can be predicted in various ways [38–46]. Such prescriptions have recently been used in global simulations of a post-merger disk [47] and CCSNe [48].

A similar analytical prediction of the flavor conversion outcome remains, so far, unrealized for “collisional” flavor instabilities (CFIs), first evidenced in [49]. CFIs take place as neutrino self-interactions combine with dif-

ferent neutrino/antineutrino reaction rates to amplify flavor coherence, contrary to the standard expectation that collisions damp flavor coherence. Linear stability analysis [50–54] for a homogeneous and isotropic background has shown the existence of different collisional-unstable modes, with resonance-like and non-resonance-like regimes. The occurrence of CFIs has been investigated in actual environments, namely CCSNe [27, 55–59] and NSMs [33, 50, 60]. However, most studies consider a simplified collision term *which only acts on flavor coherence*. This still leads to a rich phenomenology, notably with multi-energy neutrino gases, from flavor equipartition to flavor swaps [51, 52, 61–63]. Including the flavor-diagonal parts of the collision term is nevertheless important, as they lead for instance to a flavor swap in the resonance-like case [64], instead of flavor equipartition.

In this Letter, we study the non-linear outcome of collisional flavor conversion considering both classical relaxation and coherence damping components of the collision term, showing large differences with previous studies. We obtain analytical predictions of the asymptotic state that agree perfectly with numerical simulations, applying it to configurations taken from a classical NSM simulation.

Quantum Kinetic Equations—Focusing on situations where collisions play an important role on the dynamics, we restrict ourselves to isotropic neutrino distributions. Furthermore, we consider a homogeneous system, motivated by the results of [53] which show a relative dominance of the homogeneous mode of CFI. Finally, in order to make a more direct connection with some global simulations that evolve three neutrino species (ν_e , $\bar{\nu}_e$, and $\nu_x = \nu_\mu, \nu_\tau, \bar{\nu}_\mu, \bar{\nu}_\tau$) in energy-integrated schemes, we study a two-flavor, single-energy system. Under these assumptions, the evolution of the density matrix (or equivalently, the number density moment N) is given by the QKEs [65, 66]

$$\begin{aligned} \frac{dN}{dt} &= -i[H, N] + \frac{1}{2} \left\{ \begin{pmatrix} \kappa_e & 0 \\ 0 & \kappa_x \end{pmatrix}, N^{(\text{eq})} - N \right\}, \\ \frac{d\bar{N}}{dt} &= -i[\bar{H}, \bar{N}] + \frac{1}{2} \left\{ \begin{pmatrix} \bar{\kappa}_e & 0 \\ 0 & \bar{\kappa}_x \end{pmatrix}, \bar{N}^{(\text{eq})} - \bar{N} \right\}. \end{aligned} \quad (1)$$

In this equation, the Hamiltonian H is the sum of a vacuum, matter mean-field and self-interaction mean-field terms, namely, $H = H_{\text{vac}} + H_{\text{mat}} + H_{\nu\nu}$ for neutrinos and $\bar{H} = -H_{\text{vac}} + H_{\text{mat}} + H_{\nu\nu}$ for antineutrinos. The vacuum Hamiltonian reads in the flavor basis

$$H_{\text{vac}} = \frac{\omega}{2} \begin{pmatrix} -c_{2\theta} & s_{2\theta} \\ s_{2\theta} & c_{2\theta} \end{pmatrix}, \quad (2)$$

where $\omega \equiv \Delta m^2/2E_\nu$ with E_ν the common neutrino energy, and we use the compact notation $c_{2\theta} = \cos(2\theta)$ and $s_{2\theta} = \sin(2\theta)$, with θ the mixing angle. In this work, we take $\Delta m^2 = 2.5 \times 10^{-3} \text{ eV}^2$ and $\sin^2(\theta) = 0.307$ (values corresponding to Δm_{12}^2 and θ_{12} in the 3-flavor case [67]). The matter term reads, also in the flavor basis,

$$H_{\text{mat}} = \sqrt{2}G_F n_e \begin{pmatrix} 1 & 0 \\ 0 & 0 \end{pmatrix} \equiv \lambda \begin{pmatrix} 1 & 0 \\ 0 & 0 \end{pmatrix}, \quad (3)$$

where n_e is the difference of electron and positron number densities, which we express more conveniently as a function of the matter density (ρ) and the electron fraction (Y_e) through $n_e = Y_e \rho / m_u$, with $m_u \simeq 1.661 \times 10^{-24} \text{ g}$ the atomic mass unit. Finally, the self-interaction term is $H_{\nu\nu} = \sqrt{2}G_F(N - \bar{N})$. The collision term in Eq. (1) describes emission/absorption processes, with absorption opacities κ_e , $\bar{\kappa}_e$, and $\kappa_x = \bar{\kappa}_x$, the last equality requiring the absence of muons in the medium, a common assumption in simulations. Since we consider isotropic neutrino distributions, the scattering processes can be discarded. We assume that initially, the system is in the “classical” equilibrium $N(t=0) = N^{(\text{eq})} \equiv \text{diag}(N_{ee}^{(\text{eq})}, N_{xx}^{(\text{eq})})$, and likewise for antineutrinos.

Linear regime— We first establish the main features of the CFI in the linear regime, where $N_{aa} \simeq N_{aa}^{(\text{eq})}$ and $|N_{ex}| \ll 1$. Following [51], we write the ex components of the QKEs as

$$i \frac{d}{dt} \begin{bmatrix} N_{ex} \\ \bar{N}_{ex} \end{bmatrix} \simeq \frac{\omega s_{2\theta}}{2\sqrt{2}G_F} \begin{bmatrix} -\mathbf{g}^{(\text{eq})} \\ \bar{\mathbf{g}}^{(\text{eq})} \end{bmatrix} + \Lambda \begin{bmatrix} N_{ex} \\ \bar{N}_{ex} \end{bmatrix}, \quad (4)$$

where

$$\Lambda = \begin{bmatrix} -\omega c_{2\theta} + \lambda - \bar{\mathbf{g}}^{(\text{eq})} - i\Gamma & \mathbf{g}^{(\text{eq})} \\ -\bar{\mathbf{g}}^{(\text{eq})} & \omega c_{2\theta} + \lambda + \mathbf{g}^{(\text{eq})} - i\bar{\Gamma} \end{bmatrix}, \quad (5)$$

with the compact notations $\mathbf{g} \equiv \sqrt{2}G_F(N_{ee} - N_{xx})$ and $\bar{\mathbf{g}} \equiv \sqrt{2}G_F(\bar{N}_{ee} - \bar{N}_{xx})$, and the average collision rates $\Gamma \equiv (\kappa_e + \kappa_x)/2$ and $\bar{\Gamma} \equiv (\bar{\kappa}_e + \bar{\kappa}_x)/2$. The solution of Eq. (4) is

$$\begin{bmatrix} N_{ex}(t) \\ \bar{N}_{ex}(t) \end{bmatrix} = Q_0 + Q_+ e^{-i\Omega_+ t} + Q_- e^{-i\Omega_- t}, \quad (6)$$

where Q_\pm are the “plus” and “minus” eigenmodes of Λ , associated with the eigenvalues Ω_\pm , and Q_0 is set by the initial condition $N_{ex}(t=0) = \bar{N}_{ex}(t=0) = 0$. The imaginary parts of Ω_\pm , which correspond to the growth

rate of the instability if they are positive, and associated eigenvectors are (see *Supplemental Material* for details)

$$\text{Im}(\Omega_-) = \frac{\bar{\Gamma}\bar{\mathbf{g}}^{(\text{eq})} - \Gamma\mathbf{g}^{(\text{eq})}}{\mathbf{g}^{(\text{eq})} - \bar{\mathbf{g}}^{(\text{eq})}}, \quad Q_- \propto \begin{bmatrix} \mathbf{g}^{(\text{eq})} \\ \bar{\mathbf{g}}^{(\text{eq})} \end{bmatrix}, \quad (7a)$$

$$\text{Im}(\Omega_+) = \frac{\Gamma\bar{\mathbf{g}}^{(\text{eq})} - \bar{\Gamma}\mathbf{g}^{(\text{eq})}}{\mathbf{g}^{(\text{eq})} - \bar{\mathbf{g}}^{(\text{eq})}}, \quad Q_+ \propto \begin{bmatrix} 1 \\ 1 \end{bmatrix}. \quad (7b)$$

We assumed that we are outside the resonance-like regime, which is the case in the examples studied below.

NSM examples— We consider two collisional-unstable points (“A” and “B”) obtained from a general relativistic simulation of the merger of two neutron stars with component masses of $1.3 M_\odot$ and $1.4 M_\odot$ [68], specifically, from the 7 ms post-merger snapshot shown on Fig. 1 (see [45] for a discussion of FFIs in this snapshot). These points are chosen to illustrate two cases where a different branch of the CFI is unstable, namely, the minus (plus) mode for Point A (B). We detail the relevant parameters in Table I. The absorption opacities are obtained from NuLib [69] assuming the SFHo equation of state (like in the NSM simulation the data is extracted from). Given that all flux factors are smaller than 0.1, we neglect anisotropies and assume that the values N_{aa} , \bar{N}_{aa} in Table I correspond to $N_{aa}^{(\text{eq})}$, $\bar{N}_{aa}^{(\text{eq})}$.

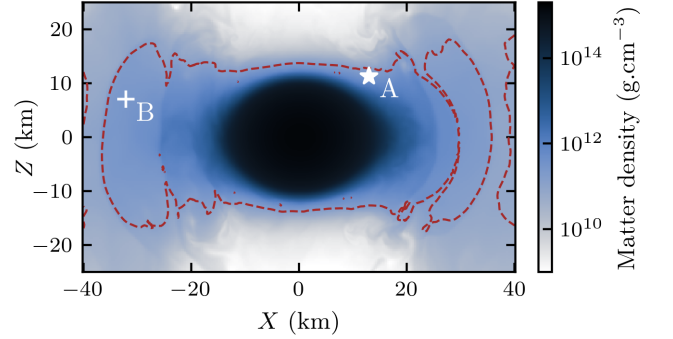


FIG. 1. Poloidal slice from the 7 ms post-merger snapshot of the “M1-NuLib” NSM simulation in [68]. The dashed line is the contour of ν_e flux factor equal to 0.1.

	Point A	Point B
$N_{ee} \text{ (cm}^{-3}\text{)}$	1.04×10^{34}	5.10×10^{33}
$\bar{N}_{ee} \text{ (cm}^{-3}\text{)}$	1.26×10^{34}	4.49×10^{33}
$N_{xx} = \bar{N}_{xx} \text{ (cm}^{-3}\text{)}$	7.10×10^{33}	1.23×10^{33}
$\rho \text{ (g.cm}^{-3}\text{)}$	2.92×10^{11}	2.50×10^{11}
Y_e	0.298	0.231
$\langle E_\nu \rangle \text{ (MeV)}$	35.7	34.6
$\kappa_e \text{ (s}^{-1}\text{)}$	7.63×10^5	2.78×10^5
$\bar{\kappa}_e \text{ (s}^{-1}\text{)}$	2.11×10^5	5.95×10^4
$\kappa_x = \bar{\kappa}_x \text{ (s}^{-1}\text{)}$	2.87×10^3	5.82×10^2

TABLE I. Conditions at points A and B identified on Fig. 1.

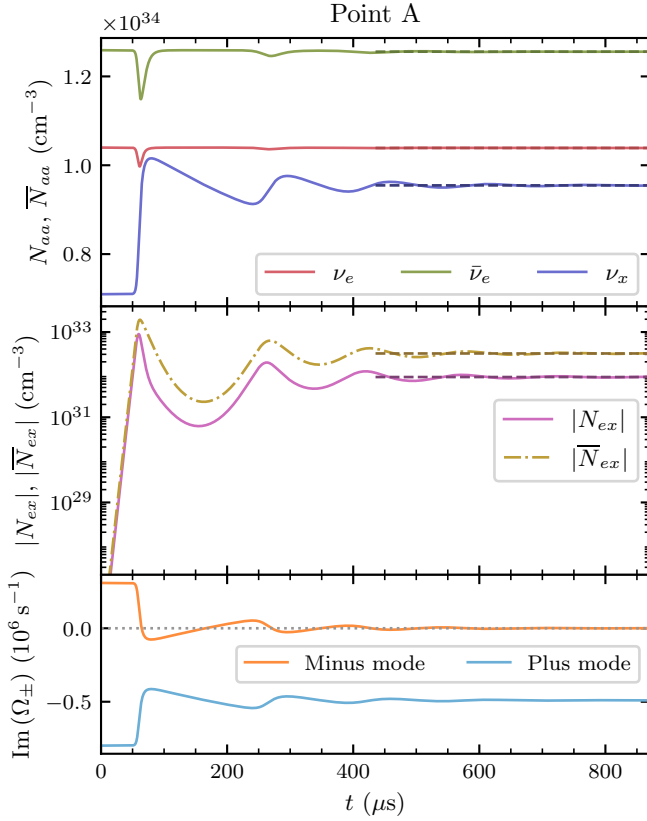


FIG. 2. Evolution of the number density flavor on-diagonal (top) and off-diagonal (middle) components for Point A. The asymptotic state predictions (see text) are shown in dashed lines. Bottom: instantaneous growth/decay rate of each instability mode, as given by Eq. (7) with $\mathbf{g}(t)$ and $\bar{\mathbf{g}}(t)$.

We solve the QKEs (1) with the explicit Runge-Kutta method of order 5(4) implemented in the function `solve_ivp` of SciPy [70]. Because of the large difference of timescales involved, we avoid numerical convergence issues by multiplying the Hamiltonian H by an attenuation factor $\eta = 10^{-3}$, but we show in the *End Matter* that the results are unaffected as long as $\eta > 10^{-4}$ (see Fig. 5). We plot the evolution of N and \bar{N} on Fig. 2 (Point A) and Fig. 3 (Point B), along with the evolution of the growth rate of each mode, as obtained from Eq. (7), at each time step of the calculation. The maximum value of $|N_{ex}|/\text{Tr}[N]$ is 0.05 (0.2) for Point A (B), which justifies to use these linear stability analysis formulas to assess the stability of each instantaneous configuration. We note that the vacuum term, which is subdominant, seeds the instability but plays no significant role otherwise, such that $N_{xx} \simeq \bar{N}_{xx}$ at all times.

For Point A, the first 100 μs correspond to the growth of the unstable minus mode (exponential growth of $|N_{ex}|$ and $|\bar{N}_{ex}|$, see middle panel), which leads to flavor conversion $\nu_e, \bar{\nu}_e \rightarrow \nu_x$. After the instability saturates, the densities of ν_e and $\bar{\nu}_e$ are repopulated very close to their classical equilibrium values, and oscillations have resulted

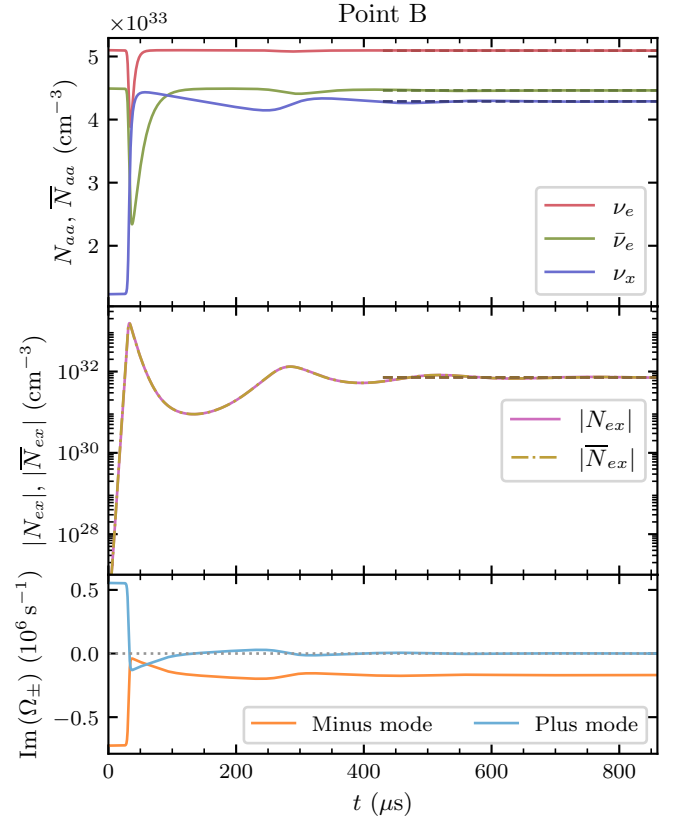


FIG. 3. Same as Fig. 2 for Point B. On the middle panel, we see that $|N_{ex}| = |\bar{N}_{ex}|$ at all times: this is a feature of the “plus” branch of the instability, consistently with the eigenvector Q_+ in Eq. (7b).

in a net increase of N_{xx} . At the end of this first phase, $N_{xx} \simeq N_{ee}$. As can be seen in the bottom panel, this configuration is stable, consistent with Eq. (7a) with $\mathbf{g} \simeq 0$. However, on a timescale $\propto \kappa_x^{-1}$, N_{xx} is drawn back toward $N_{xx}^{(\text{eq})}$, which brings the system into the unstable domain: the off-diagonal components grow again, and subsequent flavor conversion occurs, albeit with a smaller amplitude. After several cycles, the system converges toward a “quantum” equilibrium, where in particular $N_{xx} \neq N_{xx}^{(\text{eq})}$ and flavor coherence is nonzero (with $|N_{ex}|/\text{Tr}(N)$ at the percent level). For Point B, the conclusions are identical, reversing the roles of ν_e and $\bar{\nu}_e$, and the minus/plus modes. The difference of instability branches between A and B is visible in the evolutions of N_{ex} and \bar{N}_{ex} , whose different behavior is consistent with the difference between Q_- and Q_+ [see Eq. (7)].

Asymptotic state— Our goal is to analytically predict the values taken by N and \bar{N} for $t \rightarrow \infty$. More specifically, in the spirit of designing a semi-classical sub-grid model which provides a prescription for the evolution of the classical neutrino distributions (so without treating flavor coherence, even though it *is* nonzero in the final state), we want to predict the asymptotic val-

ues of the flavor-diagonal components N_{aa} and \bar{N}_{aa} . As indicated by the numerical results of Figs. 2 and 3, this asymptotic state is characterized by: (i) constant flavor-diagonal number densities, (ii) a configuration lying at the edge of collisional instability.

As stated above, the vacuum term contribution is negligible for the non-linear evolution, such that $N_{xx} \simeq \bar{N}_{xx}$ at all times. Steady-state equations for condition (i) can be written as $\text{Tr}(\dot{N}) = 0$ and $\dot{N}_{ee} - \dot{\bar{N}}_{ee} = 0$, that is,

$$\begin{aligned} \kappa_e [N_{ee}^{(\infty)} - N_{ee}^{(\text{eq})}] &= -\kappa_x [N_{xx}^{(\infty)} - N_{xx}^{(\text{eq})}], \\ \kappa_e [N_{ee}^{(\infty)} - N_{ee}^{(\text{eq})}] &= \bar{\kappa}_e [\bar{N}_{ee}^{(\infty)} - \bar{N}_{ee}^{(\text{eq})}], \end{aligned} \quad (8)$$

where we denote with a superscript (∞) the asymptotic values. Condition (ii) reads differently depending on which mode was unstable. If the system was in a “minus” instability, the final state satisfies $\text{Im}(\Omega_-^{(\infty)}) = 0$, that is,

$$\Gamma[N_{ee}^{(\infty)} - N_{xx}^{(\infty)}] = \bar{\Gamma}[\bar{N}_{ee}^{(\infty)} - N_{xx}^{(\infty)}], \quad (9)$$

while a system entering a “plus” instability reaches the final state determined by $\text{Im}(\Omega_+^{(\infty)}) = 0$, i.e.,

$$\Gamma[\bar{N}_{ee}^{(\infty)} - N_{xx}^{(\infty)}] = \bar{\Gamma}[N_{ee}^{(\infty)} - N_{xx}^{(\infty)}]. \quad (10)$$

Combining the previous equations leads to the expression for the asymptotic value of N_{ee} ,

$$\sqrt{2}G_F[N_{ee}^{(\infty)} - N_{ee}^{(\text{eq})}] = \frac{1}{\kappa_e} \frac{\bar{\Gamma}\bar{\mathbf{g}}^{(\text{eq})} - \bar{\Gamma}\mathbf{g}^{(\text{eq})}}{\Gamma\left(\frac{1}{\kappa_e} + \frac{1}{\kappa_x}\right) - \bar{\Gamma}\left(\frac{1}{\bar{\kappa}_e} + \frac{1}{\kappa_x}\right)} \quad (11)$$

for the minus instability, and

$$\sqrt{2}G_F[N_{ee}^{(\infty)} - N_{ee}^{(\text{eq})}] = \frac{1}{\kappa_e} \frac{\Gamma\bar{\mathbf{g}}^{(\text{eq})} - \bar{\Gamma}\mathbf{g}^{(\text{eq})}}{\bar{\Gamma}\left(\frac{1}{\kappa_e} + \frac{1}{\kappa_x}\right) - \Gamma\left(\frac{1}{\bar{\kappa}_e} + \frac{1}{\kappa_x}\right)} \quad (12)$$

for the plus instability. Equations (11) or (12), along with Eq. (8), fully determine the asymptotic state of the flavor-diagonal components of the density matrix. These predictions are shown as dashed lines on Figs. 2 and 3, with a perfect agreement with the numerical solution. In a semi-classical subgrid model where flavor coherence is not followed, it is thus possible to take into account CFIs through the replacement of the “equilibrium” state $N_{aa}^{(\text{eq})} \rightarrow N_{aa}^{(\infty)}$. As shown in Figs. 2 and 3, one can also predict the size of the off-diagonal component $|N_{ex}|$, which is detailed in the *End Matter* [see Eq. (18)].

Duration of relaxation— We can estimate the time required for the system to relax into the long-term quasi-steady state as follows. In the first phase post-saturation, which occurs on a timescale $\propto \text{Im}(\Omega)^{-1}$ [see Eq. (7)], ν_x adjusts to either ν_e or $\bar{\nu}_e$, which are themselves brought back approximately to their equilibrium values. We thus write $N_{xx}^{(\infty)} = \{N_{ee}^{(\text{eq})}|_-, \bar{N}_{ee}^{(\text{eq})}|_+\}$ the value of N_{xx} at the

end of this first phase (the subscript refers to the branch of instability). We crudely describe the next phase of the post-saturation period as an exponential evolution, at the rate κ_x , of N_{xx} from $N_{xx}^{(\infty)}$ toward $N_{xx}^{(\text{eq})}$, but stopped at $2N_{xx}^{(\infty)} - N_{xx}^{(\infty)}$ (symmetric value from $N_{xx}^{(\infty)}$ with respect to $N_{xx}^{(\text{eq})}$). The duration of this phase is thus¹

$$\Delta t \sim \frac{2}{\kappa_x} \frac{N_{xx}^{(\infty)} - N_{xx}^{(\text{eq})}}{N_{xx}^{(\infty)} - N_{xx}^{(\text{eq})}}, \quad (13)$$

which gives $\Delta t \simeq 180 \mu\text{s}$ for both points A and B, a value consistent with Figs. 2 and 3. In a subgrid model of flavor transformation, the prescription (11)–(12) should then be associated to a timescale of a few Δt . However, on such a large timescale, neglecting large-scale advection and the macroscopic evolution of the matter and neutrino fields is potentially problematic. It could thus be more suitable to use in a subgrid model the intermediate state $(N_{ee}^{(\text{eq})}, \bar{N}_{ee}^{(\text{eq})}, N_{xx}^{(\infty)})$ with timescale $\text{Im}(\Omega)^{-1}$. Deciding this question would require inhomogeneous simulations on larger scales, which we leave for future work.

Treatment of collisions and asymptotic state—

A key result of our study is the significant difference of final state when one includes the on-diagonal components of the collision term. To illustrate this, we plot on Fig. 4 the same quantities as in the top panel of Fig. 2, but with other implementations of collisions: neglecting κ_x (as in, e.g., [49, 61]), or keeping only the flavor off-diagonal collision term (as in, e.g., [63]). Note that the linear phase is similar in all treatments, as the flavor-diagonal components do not evolve in this phase.

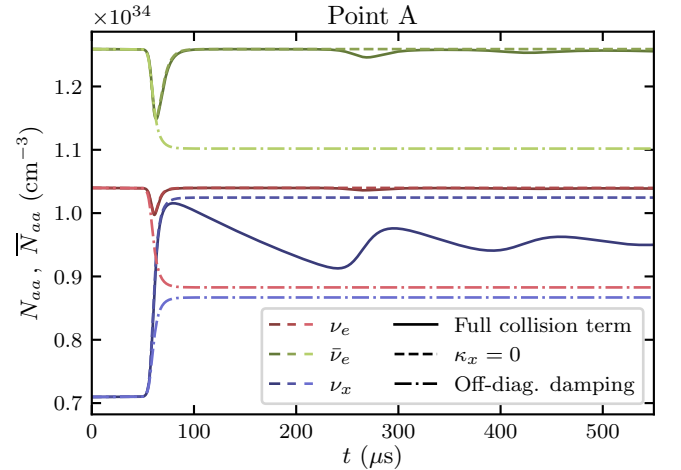


FIG. 4. Number density evolution for Point A, with different treatments of the collision term: full term as in Eq. (1) (solid lines, same as Fig. 2), ν_x opacity neglected $\kappa_x = 0$ (dashed lines), and no diagonal repopulation (dash-dotted lines). Flavor coherence is shown in the *Supplemental Material*.

¹ We approximate this portion of exponential relaxation at the rate κ_x by its linear counterpart, i.e., $e^{-\kappa_x \Delta t} \simeq 1 - \kappa_x \Delta t$.

Importantly, there is no flavor equipartition with the true collision term, as ν_e and $\bar{\nu}_e$ settle close (or exactly, if $\kappa_x = 0$) to their classical equilibrium values, far from the result obtained without diagonal collision terms, in dash-dotted lines. This incorrect treatment misses the net pair production of ν_x through the combination of $\nu_e/\bar{\nu}_e$ repopulation and oscillations. We also discuss flavor coherence and present similar conclusions for Point B in the *Supplemental Material*.

Outlook— We have studied the non-linear evolution of a neutrino/antineutrino system encountering a collisional flavor instability, deriving analytical expressions for the quasi-steady state. Notably, we have shown that studying CFIs in a setup where the effect of collisions is simply to damp the off-diagonal flavor coherence is incorrect, as it overlooks the main effect of collisions which are to drive number densities back toward their classical equilibrium values. On short timescales ($\propto \kappa_e^{-1}, \bar{\kappa}_e^{-1}$), ν_x adjusts to match ν_e or $\bar{\nu}_e$, which are close to their classical equilibria, thus resulting in a net emission of heavy-lepton flavor (anti)neutrinos. The competition between instability and classical equilibrium then leads to a “compromise” where the system lies at the edge of collisional instability, thus defining a “quantum” equilibrium. We highlight that flavor coherence is nonzero in this final state, contrary to what could naively be expected from collisions. This work provides the first explicit prediction of this asymptotic state that can be used in a subgrid model of CFIs, in spite of limitations that will need to be addressed in the future. First, we have considered monochromatic systems, thus missing the phenomenology associated with the energy dependence of collision rates (see e.g., [63]). We have also restricted our study to homogeneous and isotropic systems. Although isotropy is well-justified in the regions where CFIs will matter, inhomogeneous effects may affect the final state, in particular given the large timescales of relaxation evidenced here. These limitations form as many future directions for a more general description of CFIs in dense environments.

Acknowledgments— I thank J. Kneller, G. McLaughlin, S. Richers, F. Foucart, E. Grohs, C. Hall and E. Urquilla for many useful discussions, and in particular J. Kneller and G. McLaughlin for their valuable comments on the manuscript. This work was supported by the Network for Neutrinos, Nuclear Astrophysics and Symmetries (N3AS), through the National Science Foundation Physics Frontier Center award No. PHY-2020275.

* jfroustey@berkeley.edu

[1] H. T. Janka, T. Melson, and A. Summa, Physics of Core-Collapse Supernovae in Three Dimensions: a Sneak

- Preview, *Ann. Rev. Nucl. Part. Sci.* **66**, 341 (2016), [arXiv:1602.05576 \[astro-ph.SR\]](#).
- [2] A. Burrows and D. Vartanyan, Core-Collapse Supernova Explosion Theory, *Nature* **589**, 29 (2021), [arXiv:2009.14157 \[astro-ph.SR\]](#).
- [3] K. Kyutoku, M. Shibata, and K. Taniguchi, Coalescence of black hole-neutron star binaries, *Living Rev. Rel.* **24**, 5 (2021), [arXiv:2110.06218 \[astro-ph.HE\]](#).
- [4] D. Radice, S. Bernuzzi, and A. Perego, The Dynamics of Binary Neutron Star Mergers and GW170817, *Ann. Rev. Nucl. Part. Sci.* **70**, 95 (2020), [arXiv:2002.03863 \[astro-ph.HE\]](#).
- [5] A. Mezzacappa, Toward Realistic Models of Core Collapse Supernovae: A Brief Review, *IAU Symp.* **362**, 215 (2020), [arXiv:2205.13438 \[astro-ph.SR\]](#).
- [6] K. Kiuchi, General Relativistic Magnetohydrodynamics Simulations for Binary Neutron Star Mergers (2025) [arXiv:2405.10081 \[astro-ph.HE\]](#).
- [7] A. Mezzacappa, E. Endeve, O. E. Bronson Messer, and S. W. Bruenn, Physical, numerical, and computational challenges of modeling neutrino transport in core-collapse supernovae, *Living Rev. Comput. Astrophys.* **6**, 4 (2020), [arXiv:2010.09013 \[astro-ph.HE\]](#).
- [8] F. Foucart, Neutrino transport in general relativistic neutron star merger simulations, *Living Rev. Comput. Astrophys.* **9**, 1 (2023), [arXiv:2209.02538 \[astro-ph.HE\]](#).
- [9] T. Fischer, G. Guo, K. Langanke, G. Martinez-Pinedo, Y.-Z. Qian, and M.-R. Wu, Neutrinos and nucleosynthesis of elements, *Prog. Part. Nucl. Phys.* **137**, 104107 (2024), [arXiv:2308.03962 \[astro-ph.HE\]](#).
- [10] X. Wang and R. Surman, Neutrinos and Heavy Element Nucleosynthesis, in *Handbook of Nuclear Physics*, edited by I. Tanihata, H. Toki, and T. Kajino (Springer Nature Singapore, Singapore, 2023) pp. 1–19, [arXiv:2309.06043 \[astro-ph.HE\]](#).
- [11] H. Duan, G. M. Fuller, and Y.-Z. Qian, Collective Neutrino Oscillations, *Annu. Rev. Nucl. Part. Sci.* **60**, 569 (2010), [arXiv:1001.2799 \[hep-ph\]](#).
- [12] A. Mirizzi, I. Tamborra, H.-T. Janka, N. Saviano, K. Scholberg, R. Bollig, L. Hudepohl, and S. Chakraborty, Supernova Neutrinos: Production, Oscillations and Detection, *Riv. Nuovo Cim.* **39**, 1 (2016), [arXiv:1508.00785 \[astro-ph.HE\]](#).
- [13] S. Chakraborty, R. Hansen, I. Izaguirre, and G. Raffelt, Collective neutrino flavor conversion: Recent developments, *Nucl. Phys. B* **908**, 366 (2016), [arXiv:1602.02766 \[hep-ph\]](#).
- [14] I. Tamborra and S. Shalgar, New Developments in Flavor Evolution of a Dense Neutrino Gas, *Annu. Rev. Nucl. Part. Sci.* **71**, 165 (2021), [arXiv:2011.01948 \[astro-ph.HE\]](#).
- [15] F. Capozzi and N. Saviano, Neutrino Flavor Conversions in High-Density Astrophysical and Cosmological Environments, *Universe* **8**, 94 (2022), [arXiv:2202.02494 \[hep-ph\]](#).
- [16] M. C. Volpe, Neutrinos from dense environments: Flavor mechanisms, theoretical approaches, observations, and new directions, *Rev. Mod. Phys.* **96**, 025004 (2024), [arXiv:2301.11814 \[hep-ph\]](#).
- [17] S. Richers and M. Sen, Fast Flavor Transformations, in *Handbook of Nuclear Physics*, edited by I. Tanihata, H. Toki, and T. Kajino (Springer Nature Singapore, Singapore, 2022) pp. 1–17, [arXiv:2207.03561 \[astro-ph.HE\]](#).
- [18] L. Johns, S. Richers, and M.-R. Wu, Neutrino Oscil-

- lations in Core-Collapse Supernovae and Neutron Star Mergers, [arXiv:2503.05959 \[astro-ph.HE\]](#) (2025).
- [19] C. J. Stapleford, C. Fröhlich, and J. P. Kneller, Coupling Neutrino Oscillations and Simulations of Core-Collapse Supernovae, *Phys. Rev. D* **102**, 081301 (2020), [arXiv:1910.04172 \[astro-ph.HE\]](#).
- [20] J. Ehring, S. Abbar, H.-T. Janka, G. Raffelt, and I. Tamborra, Fast neutrino flavor conversion in core-collapse supernovae: A parametric study in 1D models, *Phys. Rev. D* **107**, 103034 (2023), [arXiv:2301.11938 \[astro-ph.HE\]](#).
- [21] J. Ehring, S. Abbar, H.-T. Janka, G. Raffelt, and I. Tamborra, Fast Neutrino Flavor Conversions Can Help and Hinder Neutrino-Driven Explosions, *Phys. Rev. Lett.* **131**, 061401 (2023), [arXiv:2305.11207 \[astro-ph.HE\]](#).
- [22] K. Mori, T. Takiwaki, K. Kotake, and S. Horiuchi, Three-dimensional core-collapse supernova models with phenomenological treatment of neutrino flavor conversions, *Publ. Astron. Soc. Jap.* **77**, L9 (2025), [arXiv:2501.15256 \[astro-ph.HE\]](#).
- [23] X. Li and D. M. Siegel, Neutrino Fast Flavor Conversions in Neutron-Star Postmerger Accretion Disks, *Phys. Rev. Lett.* **126**, 251101 (2021), [arXiv:2103.02616 \[astro-ph.HE\]](#).
- [24] O. Just, S. Abbar, M.-R. Wu, I. Tamborra, H.-T. Janka, and F. Capozzi, Fast neutrino conversion in hydrodynamic simulations of neutrino-cooled accretion disks, *Phys. Rev. D* **105**, 083024 (2022), [arXiv:2203.16559 \[astro-ph.HE\]](#).
- [25] R. Fernández, S. Richers, N. Mulyk, and S. Fahlman, Fast flavor instability in hypermassive neutron star disk outflows, *Phys. Rev. D* **106**, 103003 (2022), [arXiv:2207.10680 \[astro-ph.HE\]](#).
- [26] Y. Qiu, D. Radice, S. Richers, and M. Bhattacharyya, Neutrino Flavor Transformation in Neutron Star Mergers, [arXiv:2503.11758 \[astro-ph.HE\]](#) (2025).
- [27] Z. Xiong, M.-R. Wu, G. Martinez-Pinedo, T. Fischer, M. George, C.-Y. Lin, and L. Johns, Evolution of collisional neutrino flavor instabilities in spherically symmetric supernova models, *Phys. Rev. D* **107**, 083016 (2023), [arXiv:2210.08254 \[astro-ph.HE\]](#).
- [28] H. Nagakura and M. Zaizen, Connecting small-scale to large-scale structures of fast neutrino-flavor conversion, *Phys. Rev. D* **107**, 063033 (2023), [arXiv:2211.01398 \[astro-ph.HE\]](#).
- [29] H. Nagakura, Global features of fast neutrino-flavor conversion in binary neutron star mergers, *Phys. Rev. D* **108**, 103014 (2023), [arXiv:2306.10108 \[astro-ph.HE\]](#).
- [30] S. Shalgar and I. Tamborra, Neutrino quantum kinetics in a core-collapse supernova, *JCAP* **09**, 021, [arXiv:2406.09504 \[astro-ph.HE\]](#).
- [31] M. Myers, T. Cooper, M. Warren, J. Kneller, G. McLaughlin, S. Richers, E. Grohs, and C. Fröhlich, Neutrino flavor mixing with moments, *Phys. Rev. D* **105**, 123036 (2022), [arXiv:2111.13722 \[hep-ph\]](#).
- [32] E. Grohs, S. Richers, S. M. Couch, F. Foucart, J. P. Kneller, and G. C. McLaughlin, Neutrino fast flavor instability in three dimensions for a neutron star merger, *Phys. Lett. B* **846**, 138210 (2023), [arXiv:2207.02214 \[hep-ph\]](#).
- [33] J. Froustey, S. Richers, E. Grohs, S. D. Flynn, F. Foucart, J. P. Kneller, and G. C. McLaughlin, Neutrino fast flavor oscillations with moments: Linear stability analysis and application to neutron star mergers, *Phys. Rev. D* **109**, 043046 (2024), [arXiv:2311.11968 \[astro-ph.HE\]](#).
- [34] J. Froustey, J. P. Kneller, and G. C. McLaughlin, Quantum maximum entropy closure for small flavor coherence, *Phys. Rev. D* **111**, 063022 (2025), [arXiv:2409.05807 \[hep-ph\]](#).
- [35] J. P. Kneller, J. Froustey, E. B. Grohs, F. Foucart, G. C. McLaughlin, and S. Richers, Quantum closures for neutrino moment transport, *Phys. Rev. D* **111**, 063046 (2025), [arXiv:2410.00719 \[hep-ph\]](#).
- [36] E. Grohs, S. Richers, J. Froustey, F. Foucart, J. P. Kneller, and G. C. McLaughlin, Advection algorithms for quantum neutrino moment transport, *Phys. Rev. D* **111**, 083018 (2025), [arXiv:2501.07540 \[astro-ph.HE\]](#).
- [37] H. Nagakura, L. Johns, and M. Zaizen, Bhatnagar-Gross-Krook subgrid model for neutrino quantum kinetics, *Phys. Rev. D* **109**, 083013 (2024), [arXiv:2312.16285 \[astro-ph.HE\]](#).
- [38] S. Bhattacharyya and B. Dasgupta, Fast Flavor Depolarization of Supernova Neutrinos, *Phys. Rev. Lett.* **126**, 061302 (2021), [arXiv:2009.03337 \[hep-ph\]](#).
- [39] S. Bhattacharyya and B. Dasgupta, Elaborating the ultimate fate of fast collective neutrino flavor oscillations, *Phys. Rev. D* **106**, 103039 (2022), [arXiv:2205.05129 \[hep-ph\]](#).
- [40] M. Zaizen and H. Nagakura, Simple method for determining asymptotic states of fast neutrino-flavor conversion, *Phys. Rev. D* **107**, 103022 (2023), [arXiv:2211.09343 \[astro-ph.HE\]](#).
- [41] M. Zaizen and H. Nagakura, Characterizing quasisteady states of fast neutrino-flavor conversion by stability and conservation laws, *Phys. Rev. D* **107**, 123021 (2023), [arXiv:2304.05044 \[astro-ph.HE\]](#).
- [42] H. Nagakura and M. Zaizen, Basic characteristics of neutrino flavor conversions in the postshock regions of core-collapse supernova, *Phys. Rev. D* **108**, 123003 (2023), [arXiv:2308.14800 \[astro-ph.HE\]](#).
- [43] S. Abbar, M.-R. Wu, and Z. Xiong, Physics-informed neural networks for predicting the asymptotic outcome of fast neutrino flavor conversions, *Phys. Rev. D* **109**, 043024 (2024), [arXiv:2311.15656 \[astro-ph.HE\]](#).
- [44] Z. Xiong, M.-R. Wu, M. George, and C.-Y. Lin, Robust Integration of Fast Flavor Conversions in Classical Neutrino Transport, *Phys. Rev. Lett.* **134**, 051003 (2025), [arXiv:2403.17269 \[astro-ph.HE\]](#).
- [45] S. Richers, J. Froustey, S. Ghosh, F. Foucart, and J. Gomez, Asymptotic-state prediction for fast flavor transformation in neutron star mergers, *Phys. Rev. D* **110**, 103019 (2024), [arXiv:2409.04405 \[astro-ph.HE\]](#).
- [46] M. George, Z. Xiong, M.-R. Wu, and C.-Y. Lin, Evolution and the quasistationary state of collective fast neutrino flavor conversion in three dimensions without axisymmetry, *Phys. Rev. D* **110**, 123018 (2024), [arXiv:2409.08833 \[astro-ph.HE\]](#).
- [47] K. A. Lund, P. Mukhopadhyay, J. M. Miller, and G. C. McLaughlin, Angle-dependent in Situ Fast Flavor Transformations in Post-neutron-star-merger Disks, *Astrophys. J. Lett.* **985**, L9 (2025), [arXiv:2503.23727 \[astro-ph.HE\]](#).
- [48] T. Wang and A. Burrows, The Effect of the Fast-Flavor Instability on Core-Collapse Supernova Models, [arXiv:2503.04896 \[astro-ph.HE\]](#) (2025).
- [49] L. Johns, Collisional Flavor Instabilities of Supernova Neutrinos, *Phys. Rev. Lett.* **130**, 191001 (2023), [arXiv:2104.11369 \[hep-ph\]](#).
- [50] Z. Xiong, L. Johns, M.-R. Wu, and H. Duan, Collisional

- flavor instability in dense neutrino gases, *Phys. Rev. D* **108**, 083002 (2023), [arXiv:2212.03750 \[hep-ph\]](#).
- [51] Y.-C. Lin and H. Duan, Collision-induced flavor instability in dense neutrino gases with energy-dependent scattering, *Phys. Rev. D* **107**, 083034 (2023), [arXiv:2210.09218 \[hep-ph\]](#).
 - [52] I. Padilla-Gay, I. Tamborra, and G. G. Raffelt, Neutrino fast flavor pendulum. II. Collisional damping, *Phys. Rev. D* **106**, 103031 (2022), [arXiv:2209.11235 \[hep-ph\]](#).
 - [53] J. Liu, M. Zaizen, and S. Yamada, Systematic study of the resonancelike structure in the collisional flavor instability of neutrinos, *Phys. Rev. D* **107**, 123011 (2023), [arXiv:2302.06263 \[hep-ph\]](#).
 - [54] M. Zaizen, S. Richers, H. Nagakura, H. Suzuki, and C. Kato, Inspecting neutrino flavor instabilities during proto-neutron star cooling phase in supernova: I. Spherically symmetric model, [arXiv:2407.20548 \[astro-ph.HE\]](#) (2024).
 - [55] S. Shalgar and I. Tamborra, Do neutrinos become flavor unstable due to collisions with matter in the supernova decoupling region?, *Phys. Rev. D* **109**, 103011 (2024), [arXiv:2307.10366 \[astro-ph.HE\]](#).
 - [56] J. Liu, H. Nagakura, R. Akaho, A. Ito, M. Zaizen, and S. Yamada, Universality of the neutrino collisional flavor instability in core-collapse supernovae, *Phys. Rev. D* **108**, 123024 (2023), [arXiv:2310.05050 \[astro-ph.HE\]](#).
 - [57] R. Akaho, J. Liu, H. Nagakura, M. Zaizen, and S. Yamada, Collisional and fast neutrino flavor instabilities in two-dimensional core-collapse supernova simulation with Boltzmann neutrino transport, *Phys. Rev. D* **109**, 023012 (2024), [arXiv:2311.11272 \[astro-ph.HE\]](#).
 - [58] J. Liu, H. Nagakura, R. Akaho, A. Ito, M. Zaizen, S. Furusawa, and S. Yamada, Muon-induced collisional flavor instability in core-collapse supernova, *Phys. Rev. D* **110**, 043039 (2024), [arXiv:2407.10604 \[hep-ph\]](#).
 - [59] Z. Xiong, M.-R. Wu, M. George, C.-Y. Lin, N. K. Largani, T. Fischer, and G. Martinez-Pinedo, Fast neutrino flavor conversions in a supernova: Emergence, evolution, and effects, *Phys. Rev. D* **109**, 123008 (2024), [arXiv:2402.19252 \[astro-ph.HE\]](#).
 - [60] H. Nagakura, K. Sumiyoshi, S. Fujibayashi, Y. Sekiguchi, and M. Shibata, Neutrino flavor instabilities in a binary neutron star merger remnant: Roles of a long-lived hypermassive neutron star, [arXiv:2504.20143 \[astro-ph.HE\]](#) (2025).
 - [61] D. F. G. Fiorillo, I. Padilla-Gay, and G. G. Raffelt, Collisions and collective flavor conversion: Integrating out the fast dynamics, *Phys. Rev. D* **109**, 063021 (2024), [arXiv:2312.07612 \[hep-ph\]](#).
 - [62] L. Johns and S. Rodriguez, Collisional flavor pendula and neutrino quantum thermodynamics, [arXiv:2312.10340 \[hep-ph\]](#) (2023).
 - [63] M. Zaizen, Spectral diversity in collisional neutrino-flavor conversion: Flavor equipartition or swap, *Phys. Rev. D* **111**, 103029 (2025), [arXiv:2502.09260 \[hep-ph\]](#).
 - [64] C. Kato, H. Nagakura, and L. Johns, Collisional flavor swap with neutrino self-interactions, *Phys. Rev. D* **109**, 103009 (2024), [arXiv:2309.02619 \[astro-ph.HE\]](#).
 - [65] G. Sigl and G. Raffelt, General kinetic description of relativistic mixed neutrinos, *Nucl. Phys. B* **406**, 423 (1993).
 - [66] S. A. Richers, G. C. McLaughlin, J. P. Kneller, and A. Vlasenko, Neutrino Quantum Kinetics in Compact Objects, *Phys. Rev. D* **99**, 123014 (2019), [Erratum: *Phys. Rev. D* **109**, 129902(E) (2024)], [arXiv:1903.00022 \[astro-ph.HE\]](#).
 - [67] S. Navas *et al.* (Particle Data Group), Review of particle physics, *Phys. Rev. D* **110**, 030001 (2024).
 - [68] F. Foucart, P. C.-K. Cheong, M. D. Duez, L. E. Kidder, H. P. Pfeiffer, and M. A. Scheel, Robustness of neutron star merger simulations to changes in neutrino transport and neutrino-matter interactions, *Phys. Rev. D* **110**, 083028 (2024), [arXiv:2407.15989 \[astro-ph.HE\]](#).
 - [69] E. O'Connor, An Open-Source Neutrino Radiation Hydrodynamics Code for Core-Collapse Supernovae, *Astrophys. J. Suppl.* **219**, 24 (2015), [arXiv:1411.7058 \[astro-ph.HE\]](#).
 - [70] P. Virtanen *et al.*, SciPy 1.0: Fundamental Algorithms for Scientific Computing in Python, *Nature Methods* **17**, 261 (2020).
 - [71] J. Froustey, C. Pitrou, and M. C. Volpe, Neutrino decoupling including flavour oscillations and primordial nucleosynthesis, *JCAP* **12**, 015, [arXiv:2008.01074 \[hep-ph\]](#).
 - [72] J. Froustey and C. Pitrou, Primordial neutrino asymmetry evolution with full mean-field effects and collisions, *JCAP* **03** (03), 065, [arXiv:2110.11889 \[hep-ph\]](#).

End Matter

Attenuation of the Hamiltonian— As mentioned in the main text, for computational reasons we use an attenuated Hamiltonian, where the vacuum, matter and self-interaction contributions in Eq. (1) are multiplied by an attenuation factor² $\eta < 1$. This is necessary in practice because the matter term in particular introduces an extremely small timescale (see Table II). In addition, the matter term reduces the amplitude of the eigenvectors Q_{\pm} in Eq. (6), see Eq. (12) in [51] with the expressions of Ω_{\pm} given in the *Supplemental Material*, thus requiring exceedingly small error tolerances in the ODE solver.

	Point A	Point B
$\sqrt{2}G_F N_{ee} - \bar{N}_{ee} \text{ (s}^{-1}\text{)}$	4.2×10^{11}	1.2×10^{11}
$\sqrt{2}G_F n_e \text{ (s}^{-1}\text{)}$	1.0×10^{13}	6.9×10^{12}
$\Delta m^2/2\langle E_{\nu} \rangle \text{ (s}^{-1}\text{)}$	5.3×10^4	5.5×10^4

TABLE II. Frequencies involved in Eq. (1) for the conditions of the points in Table I, where the collision rates are reported.

We observe from Fig. 5 that using $\eta > 10^{-4}$ does not change the evolution and in particular the final state equilibrium; we are then safely in the regime where the collision timescale is much larger than the self-interaction (and matter) timescales. Ideally, one could circumvent this procedure by tracking only the “slow” evolution driven by collisions (which have secular effects on the very fast oscillations happening on matter/self-interaction timescales), following strategies which leverage the large timescale separation, such as the adiabatic-like approximation in [71, 72], the coarse-graining of [62] or the “slow-dynamics equations” derived in [61].

Magnitude of flavor coherence— We introduce the modulus and phase of the flavor off-diagonal component of the density matrix, specifically:

$$\begin{aligned} N_{ex} &\equiv R e^{iS}, & R > 0, & 0 \leq S < 2\pi, \\ \bar{N}_{ex} &\equiv \bar{R} e^{i\bar{S}}, & \bar{R} > 0, & 0 \leq \bar{S} < 2\pi, \end{aligned} \quad (14)$$

and we define the phase difference $\Delta S \equiv \bar{S} - S$. The evolution of N_{ex} and \bar{N}_{ex} can thus be written

$$\dot{R} = -\Gamma R + \mathbf{g} \bar{R} \sin(\Delta S), \quad (15a)$$

$$R \dot{S} = (\omega c_{2\theta} - \lambda)R - \mathbf{g} \bar{R} \cos(\Delta S) + \bar{\mathbf{g}} R, \quad (15b)$$

$$\dot{\bar{R}} = -\bar{\Gamma} \bar{R} + \bar{\mathbf{g}} R \sin(\Delta S), \quad (15c)$$

$$\bar{R} \dot{\bar{S}} = (-\omega c_{2\theta} - \lambda)\bar{R} + \bar{\mathbf{g}} R \cos(\Delta S) - \mathbf{g} \bar{R}. \quad (15d)$$

² Note that this approach is slightly different from the one in, e.g., [27, 30], where only the self-interaction Hamiltonian is rescaled.

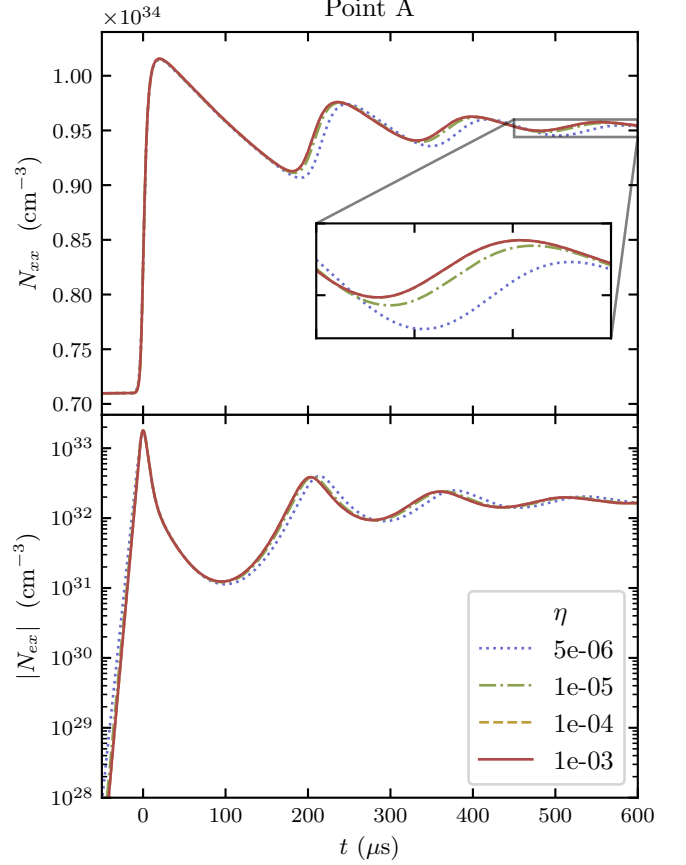


FIG. 5. Modification of the evolution for different attenuation factors η in the Hamiltonian (see text). There is no discernible difference for attenuations larger than 10^{-4} , where we are safely in the regime $\Gamma \ll \|H\|$.

The evolution of N_{ee} reads, in terms of moduli and phases of the off-diagonal components and neglecting the vacuum term,

$$\dot{N}_{ee} = -2\sqrt{2}G_F R \bar{R} \sin(\Delta S) - \kappa_e [N_{ee} - N_{ee}^{(eq)}]. \quad (16)$$

In the main text, we have defined the post-CFI asymptotic state based on the constancy of the flavor-diagonal components, and a “threshold of instability” condition. We can revisit this latter feature based on the following observations. When considering the off-diagonal components, the asymptotic state is further characterized by the constancy of the magnitudes R, \bar{R} . In addition, the ratio R/\bar{R} remains determined by the unstable eigenvector Q_{\pm} throughout the evolution, which is confirmed in Fig. 6 for both Points A [top panel, ratio R/\bar{R} equal at all times to $\mathbf{g}/\bar{\mathbf{g}}$, consistent with Eq. (7a)] and B [bottom panel, ratio $R/\bar{R} = 1$, consistent with Eq. (7b)]. At small times, the large scatter of R/\bar{R} corresponds to the system settling into the unstable mode.

The asymptotic state thus satisfies the following set of

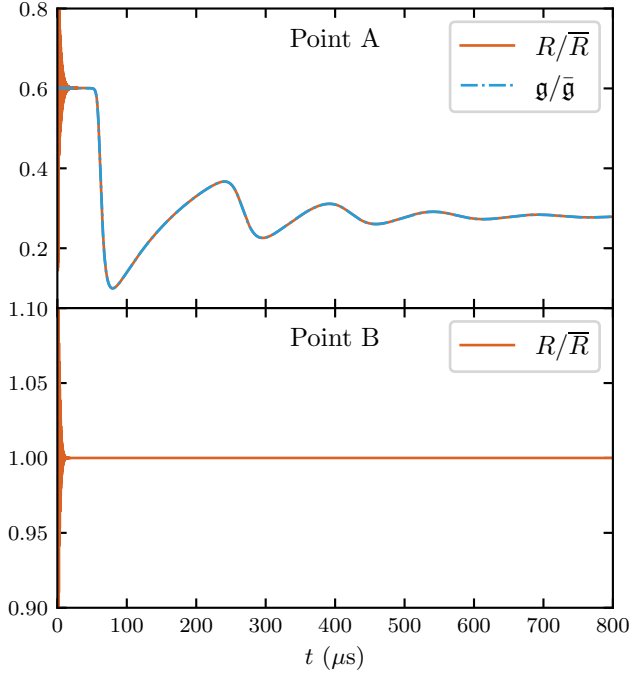


FIG. 6. Conservation of the unstable eigenvector structure in flavor coherence for the two points studied. *Top*: point A, where the minus mode is unstable. *Bottom*: point B, where the plus mode is unstable. The ratio R/\bar{R} follows the ratio of components of Q_{\pm} , see Eq. (7).

equations:

$$\kappa_e [N_{ee}^{(\infty)} - N_{ee}^{(\text{eq})}] = -\kappa_x [N_{xx}^{(\infty)} - N_{xx}^{(\text{eq})}], \quad (17a)$$

$$\kappa_e [N_{ee}^{(\infty)} - N_{ee}^{(\text{eq})}] = \bar{\kappa}_e [\bar{N}_{ee}^{(\infty)} - \bar{N}_{ee}^{(\text{eq})}], \quad (17b)$$

$$\kappa_e [N_{ee}^{(\infty)} - N_{ee}^{(\text{eq})}] = -2\sqrt{2}G_F R^{(\infty)} \bar{R}^{(\infty)} \sin[\Delta S^{(\infty)}], \quad (17c)$$

$$\Gamma R^{(\infty)} = \sqrt{2}G_F [N_{ee}^{(\infty)} - N_{xx}^{(\infty)}] \bar{R}^{(\infty)} \sin[\Delta S^{(\infty)}], \quad (17d)$$

$$\bar{\Gamma} \bar{R}^{(\infty)} = \sqrt{2}G_F [\bar{N}_{ee}^{(\infty)} - N_{xx}^{(\infty)}] R^{(\infty)} \sin[\Delta S^{(\infty)}], \quad (17e)$$

$$\frac{R^{(\infty)}}{\bar{R}^{(\infty)}} = \begin{cases} \frac{N_{ee}^{(\infty)} - N_{xx}^{(\infty)}}{\bar{N}_{ee}^{(\infty)} - N_{xx}^{(\infty)}} & (\text{minus mode}), \\ 1 & (\text{plus mode}). \end{cases} \quad (17f)$$

The ratio of Eqs. (17d) and (17e), combined with Eq. (17f), leads to the instability threshold conditions (9) (minus case) and (10) (plus case). Finally, inserting Eq. (17d) in Eq. (17c) leads to the prediction for the amount of flavor coherence in the asymptotic state:

$$R^{(\infty)} = \sqrt{-\frac{\kappa_e}{\kappa_e + \kappa_x} [N_{ee}^{(\infty)} - N_{ee}^{(\text{eq})}] [N_{ee}^{(\infty)} - N_{xx}^{(\infty)}]}. \quad (18)$$

The same expression in the antineutrino sector is obtained via Eq. (17f). We can show that the argument of the square root in Eq. (18) is positive, focusing for


simplicity on the relevant case $\kappa_x \ll \kappa_e, \bar{\kappa}_e$. We then have

$$\left[R_{\pm}^{(\infty)} \right]^2 \simeq \frac{2\alpha_{\pm}\kappa_x}{(\kappa_e - \bar{\kappa}_e)^2} \text{Im}(\Omega_{\pm}) \left[N_{ee}^{(\text{eq})} - \bar{N}_{ee}^{(\text{eq})} \right]^2, \quad (19)$$

with $\alpha_+ = 1$ and $\alpha_- = \kappa_e/\bar{\kappa}_e$, and the growth rate of the instability is given by Eq. (7). Since by definition, $\text{Im}(\Omega_{\pm}) > 0$ if there is an instability, this ensures that the right-hand side of Eq. (19) is positive.

The prediction (18) is shown on the middle panels of Figs. 2–3, in perfect agreement with the numerical solution of the QKEs. Importantly, these final values are not vanishingly small, which would have been the case with an incomplete version of the collision term (see *Supplemental Material*).

Supplemental Material for Predicting the outcome of collisional neutrino flavor conversion

Julien Froustey ^{1,2,*}

¹*Department of Physics, University of California Berkeley, Berkeley, CA 94720, USA*

³*Department of Physics, University of California San Diego, La Jolla, CA 92093, USA*

We provide material that is not needed to understand the primary message of our work, giving detailed expressions for the evolution equations, deriving the linear stability analysis results used in the main text and expanding the discussion on different implementations of collisional processes in the QKE.

Quantum Kinetic Equations

We reproduce here the explicit, component-by-component version of the QKEs (1).

$$\frac{dN_{ee}}{dt} = -s_{2\theta} \omega \operatorname{Im}(N_{ex}) + 2\sqrt{2}G_F \operatorname{Im}(N_{ex}\bar{N}_{ex}^*) - \kappa_e (N_{ee} - N_{ee}^{(\text{eq})}) , \quad (\text{S.1a})$$

$$\frac{dN_{xx}}{dt} = +s_{2\theta} \omega \operatorname{Im}(N_{ex}) - 2\sqrt{2}G_F \operatorname{Im}(N_{ex}\bar{N}_{ex}^*) - \kappa_x (N_{xx} - N_{xx}^{(\text{eq})}) , \quad (\text{S.1b})$$

$$\frac{d\bar{N}_{ee}}{dt} = +s_{2\theta} \omega \operatorname{Im}(\bar{N}_{ex}) + 2\sqrt{2}G_F \operatorname{Im}(N_{ex}\bar{N}_{ex}^*) - \bar{\kappa}_e (\bar{N}_{ee} - \bar{N}_{ee}^{(\text{eq})}) , \quad (\text{S.1c})$$

$$\frac{d\bar{N}_{xx}}{dt} = -s_{2\theta} \omega \operatorname{Im}(\bar{N}_{ex}) - 2\sqrt{2}G_F \operatorname{Im}(N_{ex}\bar{N}_{ex}^*) - \bar{\kappa}_x (\bar{N}_{xx} - \bar{N}_{xx}^{(\text{eq})}) , \quad (\text{S.1d})$$

$$\frac{dN_{ex}}{dt} = i c_{2\theta} \omega N_{ex} - i \lambda N_{ex} + i \frac{s_{2\theta}}{2} \omega (N_{ee} - N_{xx}) - i \sqrt{2}G_F [(N_{ee} - N_{xx})\bar{N}_{ex} - (\bar{N}_{ee} - \bar{N}_{xx})N_{ex}] - \frac{\kappa_e + \kappa_x}{2} N_{ex} , \quad (\text{S.1e})$$

$$\frac{d\bar{N}_{ex}}{dt} = -i c_{2\theta} \omega \bar{N}_{ex} - i \lambda \bar{N}_{ex} - i \frac{s_{2\theta}}{2} \omega (\bar{N}_{ee} - \bar{N}_{xx}) - i \sqrt{2}G_F [(N_{ee} - N_{xx})\bar{N}_{ex} - (\bar{N}_{ee} - \bar{N}_{xx})N_{ex}] - \frac{\bar{\kappa}_e + \bar{\kappa}_x}{2} \bar{N}_{ex} . \quad (\text{S.1f})$$

One can also use the polarization vector formalism, writing $N = \frac{1}{2} (P_0 \mathbb{I} + \mathbf{P} \cdot \boldsymbol{\sigma})$, with $\boldsymbol{\sigma} = (\sigma_x, \sigma_y, \sigma_z)^T$ the “vector” of Pauli matrices. This representation leads to the correspondences

$$P_0 = N_{ee} + N_{xx} , \quad P_x = 2 \operatorname{Re}(N_{ex}) , \quad P_y = -2 \operatorname{Im}(N_{ex}) , \quad P_z = N_{ee} - N_{xx} . \quad (\text{S.2})$$

The QKEs then become precession equations for \mathbf{P} and $\bar{\mathbf{P}}$, with extra features due to collisions (which also change P_0 and \bar{P}_0), namely,

$$\dot{P}_0 = \frac{\kappa_e + \kappa_x}{2} (P_0^{(\text{eq})} - P_0) + \frac{\kappa_e - \kappa_x}{2} (P_z^{(\text{eq})} - P_z) , \quad (\text{S.3a})$$

$$\dot{\mathbf{P}} = +\omega \mathbf{B} \times \mathbf{P} + \lambda \hat{\mathbf{z}} \times \mathbf{P} + \sqrt{2}G_F (\mathbf{P} - \bar{\mathbf{P}}) \times \mathbf{P} + \left[\frac{\kappa_e + \kappa_x}{2} (P_z^{(\text{eq})} - P_z) + \frac{\kappa_e - \kappa_x}{2} (P_0^{(\text{eq})} - P_0) \right] \hat{\mathbf{z}} - \frac{\kappa_e + \kappa_x}{2} \mathbf{P}_\perp , \quad (\text{S.3b})$$

$$\dot{\bar{P}}_0 = \frac{\bar{\kappa}_e + \bar{\kappa}_x}{2} (\bar{P}_0^{(\text{eq})} - \bar{P}_0) + \frac{\bar{\kappa}_e - \bar{\kappa}_x}{2} (\bar{P}_z^{(\text{eq})} - \bar{P}_z) , \quad (\text{S.3c})$$

$$\dot{\bar{\mathbf{P}}} = -\omega \mathbf{B} \times \bar{\mathbf{P}} + \lambda \hat{\mathbf{z}} \times \bar{\mathbf{P}} + \sqrt{2}G_F (\mathbf{P} - \bar{\mathbf{P}}) \times \bar{\mathbf{P}} + \left[\frac{\bar{\kappa}_e + \bar{\kappa}_x}{2} (\bar{P}_z^{(\text{eq})} - \bar{P}_z) + \frac{\bar{\kappa}_e - \bar{\kappa}_x}{2} (\bar{P}_0^{(\text{eq})} - \bar{P}_0) \right] \hat{\mathbf{z}} - \frac{\bar{\kappa}_e + \bar{\kappa}_x}{2} \bar{\mathbf{P}}_\perp , \quad (\text{S.3d})$$

with $\mathbf{B} = (s_{2\theta}, 0, -c_{2\theta})^T$, $\hat{\mathbf{z}} = (0, 0, 1)^T$, $\mathbf{P}_\perp = (P_x, P_y, 0)^T$, $P_0^{(\text{eq})} = N_{ee}^{(\text{eq})} + N_{xx}^{(\text{eq})}$ and $P_z^{(\text{eq})} = N_{ee}^{(\text{eq})} - N_{xx}^{(\text{eq})}$ (and similarly for antineutrinos).

* jfroustey@berkeley.edu

Linear stability analysis

We detail here the results of the linear stability analysis of the system described by Eq. (1). To make the connection with other works in the literature, specifically [53, 54, 56–58, 63], we introduce the notations

$$\begin{aligned} G &\equiv \frac{\mathfrak{g} + \bar{\mathfrak{g}}}{2}, & \gamma &\equiv \frac{\Gamma + \bar{\Gamma}}{2}, \\ A &\equiv \frac{\mathfrak{g} - \bar{\mathfrak{g}}}{2}, & \alpha &\equiv \frac{\Gamma - \bar{\Gamma}}{2}. \end{aligned} \quad (\text{S.4})$$

Throughout this section, we drop the (eq) exponents which are implicit.

Neglecting the vacuum contribution, the stability matrix in Eq. (4) can be rewritten

$$\Lambda = \begin{bmatrix} A - G - i(\alpha + \gamma) - \omega c_{2\theta} + \lambda & A + G \\ A - G & A + G - i(\alpha + \gamma) + \omega c_{2\theta} + \lambda \end{bmatrix}. \quad (\text{S.5})$$

Its eigenvalues and eigenvectors are[†]

$$\begin{aligned} Q_1 &= \begin{bmatrix} G + i\alpha + \sqrt{A^2 + 2iG\alpha - \alpha^2} \\ G - A \end{bmatrix}, & \Omega_1 &= \lambda + A - \sqrt{A^2 + (i\alpha + \omega c_{2\theta})(2G + i\alpha + \omega c_{2\theta})} - i\gamma, \\ Q_2 &= \begin{bmatrix} G + i\alpha - \sqrt{A^2 + 2iG\alpha - \alpha^2} \\ G - A \end{bmatrix}, & \Omega_2 &= \lambda + A + \sqrt{A^2 + (i\alpha + \omega c_{2\theta})(2G + i\alpha + \omega c_{2\theta})} - i\gamma. \end{aligned} \quad (\text{S.6})$$

Outside of the resonance-like regime, we have $|G\alpha| \ll A^2$ (and also $|\alpha| \ll G$, $|\omega c_{2\theta}| \ll G$), which allows to simplify the expressions as

$$\begin{aligned} Q_1 &\simeq \begin{bmatrix} G + |A| \\ G - A \end{bmatrix}, & \Omega_1 &\simeq \lambda + (A - |A|) - \frac{G\omega c_{2\theta}}{|A|} + i\left(-\gamma - \frac{G\alpha}{|A|}\right), \\ Q_2 &\simeq \begin{bmatrix} G - |A| \\ G - A \end{bmatrix}, & \Omega_2 &\simeq \lambda + (A + |A|) + \frac{G\omega c_{2\theta}}{|A|} + i\left(-\gamma + \frac{G\alpha}{|A|}\right). \end{aligned} \quad (\text{S.7})$$

Depending on the sign of the various quantities, we always have an eigenmode (the “minus” mode)

$$\begin{aligned} Q_- &\simeq \begin{bmatrix} G + A \\ G - A \end{bmatrix} = \begin{bmatrix} \mathfrak{g} \\ \bar{\mathfrak{g}} \end{bmatrix} \quad \text{with eigenvalue} \quad \Omega_- \simeq \lambda - \frac{G\omega c_{2\theta}}{A} + i\left(-\gamma - \frac{G\alpha}{A}\right) \\ &= \lambda - \frac{\mathfrak{g} + \bar{\mathfrak{g}}}{\mathfrak{g} - \bar{\mathfrak{g}}} \omega c_{2\theta} + i \frac{\bar{\Gamma}\bar{\mathfrak{g}} - \Gamma\mathfrak{g}}{\mathfrak{g} - \bar{\mathfrak{g}}}, \end{aligned} \quad (\text{S.8})$$

in agreement with Eq. (14) in [51]. The other eigenmode (the “plus” mode) is, after multiplying the eigenvector by $(G - A)^{-1}$,

$$\begin{aligned} Q_+ &\simeq \begin{bmatrix} 1 \\ 1 \end{bmatrix} \quad \text{with eigenvalue} \quad \Omega_+ \simeq \lambda + \frac{G\omega c_{2\theta}}{A} + 2A + i\left(-\gamma + \frac{G\alpha}{A}\right) \\ &= \lambda + \frac{\mathfrak{g} + \bar{\mathfrak{g}}}{\mathfrak{g} - \bar{\mathfrak{g}}} \omega c_{2\theta} + \mathfrak{g} - \bar{\mathfrak{g}} + i \frac{\Gamma\bar{\mathfrak{g}} - \bar{\Gamma}\mathfrak{g}}{\mathfrak{g} - \bar{\mathfrak{g}}}, \end{aligned} \quad (\text{S.9})$$

in agreement with Eq. (13) in [51]. The imaginary parts of Eqs. (S.8)–(S.9) are given in the main text, Eq. (7).

We decide here to designate the “plus/minus” mode depending on the expression of the eigenvector. Indeed, this is a *physical* distinction (see e.g., [18, 61] for further discussions). In the polarization vector formalism, the minus mode corresponds to a collective transverse growth of \mathbf{P} and $\bar{\mathbf{P}}$, which are “locked” on $\mathbf{P} - \bar{\mathbf{P}}$; in other words their common axis of precession tilts away from $\hat{\mathbf{z}}$. For the plus mode, the axis of precession remains essentially $\hat{\mathbf{z}}$, but the aperture of the precession cones grows exponentially, with \mathbf{P} and $\bar{\mathbf{P}}$ “blooming” and developing large transverse components.

[†] Some references define shifted frequencies $\Omega' \equiv \Omega - 2A - \lambda$, such that the real parts of the eigenvalues can appear different

between various sources, while the imaginary parts remain the same.

Collision term implementation

In this section, we expand the discussion on the different possible treatments of collisions, outlined in the main text around Fig. 4. We plot on Fig. A the evolution of the system for Points A (left) and B (right) under different assumptions, as in Fig. 4: solid lines for the baseline case, dashed lines taking $\kappa_x = \bar{\kappa}_x = 0$, and dash-dotted lines keeping only flavor off-diagonal damping (i.e., in the polarization vector formalism, taking $\dot{P}_0 = \dot{\bar{P}}_0 = 0$ and retaining only the transverse damping term in the collision part of $\dot{\mathbf{P}}$ and $\dot{\bar{\mathbf{P}}}$).

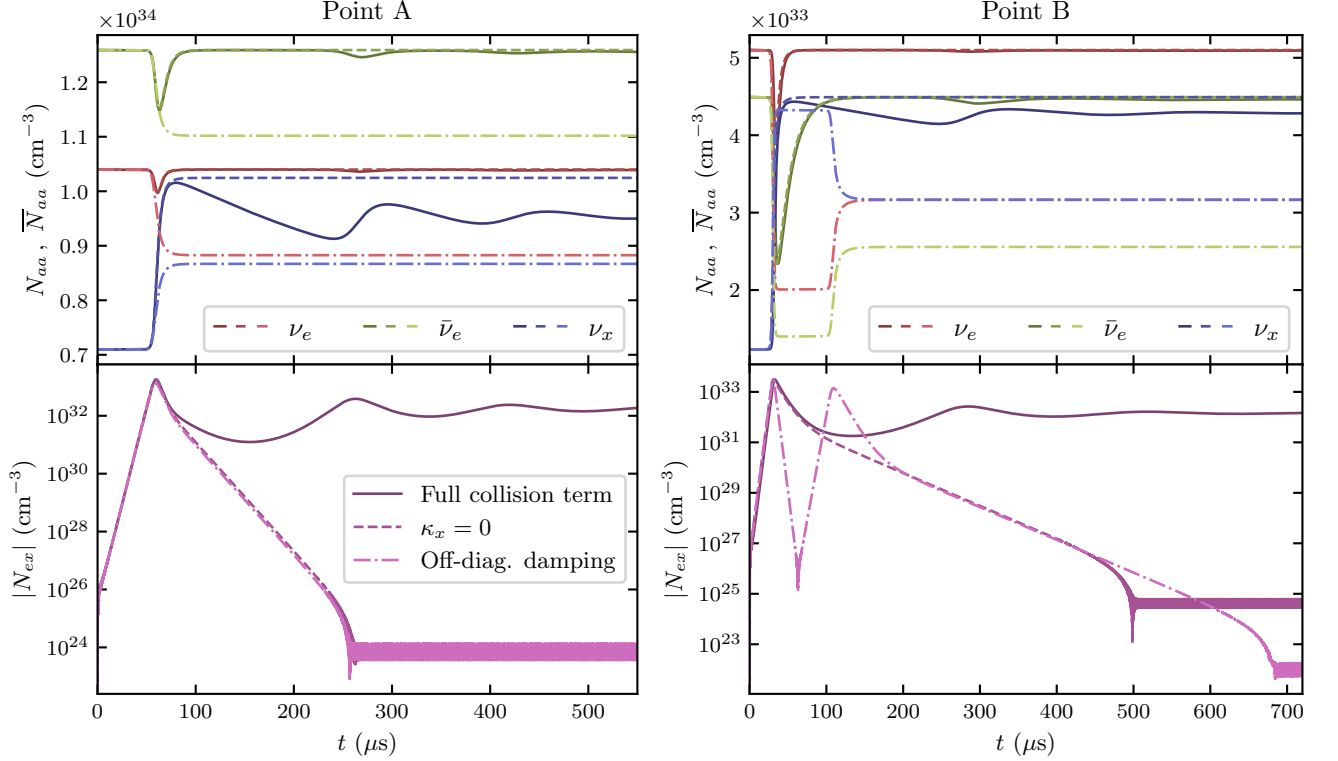


FIG. A. Dependence of neutrino evolution on the treatment of the collision term, for Point A (left) and Point B (right). The top left panel is identical to Fig. 4. On the bottom panels, we only represent the neutrino off-diagonal component for clarity.

For both points, if the xx entry of the collision term is zero (whether $\kappa_x = 0$ or whether there is only off-diagonal damping), the final amount of flavor coherence is zero up to a small contribution due to the vacuum term. If the on-diagonal terms are kept for ν_e and $\bar{\nu}_e$, Eq. (8) shows that the asymptotic state is $N_{ee} = N_{ee}^{(\text{eq})}$ and $\bar{N}_{ee} = \bar{N}_{ee}^{(\text{eq})}$. For Point A, the final value of N_{xx} is dictated by an approximate flavor “equalization” with ν_e . If $\kappa_x = 0$, then $N_{xx} \simeq N_{ee}^{(\text{eq})} = N_{xx}^{(=)}$, consistently with the discussion around Eq. (13) (since the “true” asymptotic state $N_{xx}^{(\infty)}$ is pushed to $t \rightarrow +\infty$ as $\kappa_x \rightarrow 0$). If there is only flavor off-diagonal damping, we recover the usual flavor equipartition discussed in other works (see, e.g., [51, 62, 63]), and \bar{N}_{ee} is set by the conservation of $\text{Tr}(\bar{N})$ (since there are no on-diagonal collision terms that can change the trace).

For Point B, the evolution in the $\kappa_x = 0$ case is easy to understand and similar to Point A: after the saturation of the instability, N_{xx} remains stuck on $N_{xx}^{(=)} = \bar{N}_{ee}^{(\text{eq})}$, and N_{ee} and \bar{N}_{ee} are back to their classical equilibrium values. The evolution in the “off-diagonal damping only” case is more subtle. At first, following the plus instability, there is a flavor swap between ν_x and $\bar{\nu}_e$ (see the almost perfect inversion of the dash-dotted blue and green lines) in the first 100 μs . However, this new configuration is unstable, but for the *minus* mode, while the plus mode is stable (with a negative imaginary part). This is the reason why $|N_{ex}|$ first decreases, as the plus mode decays, before the newly unstable minus mode takes over and leads to a second instability, this time inducing the equipartition of ν_x and ν_e . With the “full” collision term, this change of unstable mode is prevented by the fact that N_{ee} and \bar{N}_{ee} remain close to their classical equilibrium values.

Interestingly, the outcome (swap/equipartition) of the “off-diagonal damping only” CFI is related to which mode (plus/minus) is unstable, as noted in [63]—although this work used multi-energy distributions.